Timing Dissociative Ionization of H_2 Using a Polarization-Skewed Femtosecond Laser Pulse

Qinying Ji,[1] Shengzhe Pan,[1] Peilun He,[2] Junping Wang,[2] Peifen Lu,[1] Hui Li,[1] Xiaochun Gong,[1] Kang Lin,[1] Wenbin Zhang,[1] Junyang Ma,[1] Hanxiao Li,[1] Chungang Duan,[1] Peng Liu,[3] Ya Bai,[3] Ruxin Li,[3] Feng He,[2,*] and Jian Wu[1,4,†]

[1]*State Key Laboratory of Precision Spectroscopy, East China Normal University, Shanghai 200062, China*

[2]*Key Laboratory for Laser Plasmas (Ministry of Education) and School of Physics and Astronomy, Collaborative Innovation Center of IFSA (CICIFSA), Shanghai Jiao Tong University, Shanghai 200240, China*

[3]*State Key Laboratory of High Field Laser Physics, Shanghai Institute of Optics and Fine Mechanics, Chinese Academy of Sciences, Shanghai 201800, China*

[4]*Collaborative Innovation Center of Extreme Optics, Shanxi University, Taiyuan, Shanxi 030006, China*

(Received 15 March 2019; revised manuscript received 9 November 2019; published 4 December 2019)

We experimentally observe the bond stretching time of one-photon and net-two-photon dissociation pathways of singly ionized H_2 molecules driven by a polarization-skewed femtosecond laser pulse. By measuring the angular distributions of the ejected photoelectron and nuclear fragments in coincidence, the cycle-changing polarization of the laser field enables us to clock the photon-ionization starting time and photon-dissociation stopping time, analogous to a stopwatch. After the single ionization of H_2, our results show that the produced H_2^+ takes almost the same time in the one-photon and net-two-photon dissociation pathways to stretch to the internuclear distance of the one-photon coupled dipole-transition between the ground and excited electronic states. The spatiotemporal mapping character of the polarization-skewed laser field provides us a straightforward route to clock the ultrafast dynamics of molecules with sub-optical-cycle time resolution.

DOI: 10.1103/PhysRevLett.123.233202

As the simplest molecule in nature, H_2 serves as a prototype for exploring numerous fundamental phenomena in strong-field physics, which stands as the cornerstone for understanding the breakage of molecular bonds [1–3], the intramolecular electron localization [4–10], the charge resonance enhanced ionization of molecules [11–16], the absorption and deposition of the photon energy in molecules [17–20], the Rydberg state excitation of breaking molecules [21,22], and the Young's double-slit interference of electron wave packet [23,24]. In particular, the dissociative single ionization of H_2 plays the role of initiator in most of the above-mentioned strong-field phenomena, where one of the two valence electrons may be stripped off and the newborn H_2^+ will dissociate by absorbing extra photons from the remaining laser field, i.e., $H_2 + nh\omega \rightarrow H^+ + H + e$, denoted as the $H_2(1,0)$ channel.

As illustrated in Fig. 1(a), H_2 is ionized at the equilibrium internuclear distance R_{equ}. The produced H_2^+ may afterward dissociate via either the one-photon (labeled as ω) or the net-two-photon [labeled as $(3\text{–}1)\omega$] dissociation pathway, which brings different kinetic energy releases (KERs) of the ejected nuclear fragments [25–28]. In the one-photon pathway, H_2^+ is resonantly excited to the $2p\sigma_u^+$ state from the $1s\sigma_g^+$ state by absorbing one photon at the internuclear distance of R_ω, followed by dissociation on the $2p\sigma_u^+$ curve, as guided by the red arrows in Fig. 1(a). The situation becomes complicated when it undergoes the net-two-photon dissociation pathway. As guided by the blue arrows, H_2^+ may transit to the $2p\sigma_u^+$ state at the internuclear distance of $R_{3\omega}$ by absorbing three photons followed by propagation on the $2p\sigma_u^+$ curve until reaching R_ω, where the H_2^+ is dumped back to the $1s\sigma_g^+$ state by emitting one photon and finally dissociates on the $1s\sigma_g^+$ curve. Although these two dissociation pathways have been intensively investigated, the temporal evolution of these ultrafast processes is yet unclear. A natural question would be whether it is possible to track in real time the dissociation process, for instance, answering in which pathway H_2^+ will reach R_ω faster after the photoionization of H_2 at R_{equ}. Timing the dissociation process will allow us to figure out precisely the phase accumulation of different pathways during the bond stretching process, which governs various interesting scenarios in molecular systems such as the interference of electronic and nuclear wave packets [19].

The pump-probe scheme of ultrashort laser pulses [29–32] is generally used to time the ultrafast processes, but in that scheme, the time resolution is limited by the pulse duration which is usually several optical cycles. On the other hand, the angular streaking technique [2,33–35] using a circularly or elliptically polarized laser pulse can provide attosecond time resolution, but with this technique, it is hard to distinguish events from neighboring optical cycles of the multicycle laser pulse. In this Letter, we construct a stopwatch experimentally using a polarization-skewed femtosecond laser pulse with sub-optical-cycle time resolution and use it to observe the bond stretching

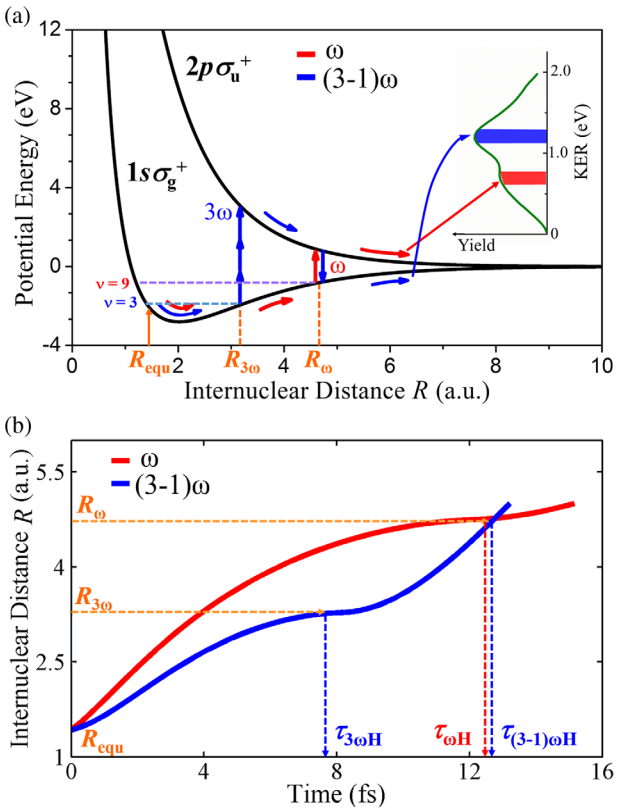

FIG. 1. (a) The $1s\sigma_g^+$ and $2p\sigma_u^+$ potential energy curves of H_2^+. The red and blue arrows illustrate the one-photon and net-two-photon dissociation pathways, respectively. The dashed horizontal lines indicate the vibrational states of $\nu = 3$ and $\nu = 9$ on the $1s\sigma_g^+$ potential energy curve. The inset (green curve) shows the measured KER spectrum of the $H_2(1,0)$ channel, where the highlighted red and blue areas correspond to the one-photon and net-two-photon dissociation pathways, respectively. (b) The time-dependent internuclear distance of the stretching H_2^+ simulated by our classical model for the one-photon (red curve) and net-two-photon (blue curve) dissociation pathways.

time of different dissociative ionization pathways of H_2. Our results show that the H_2^+ wave packet launched by photoionization spends the same time stretching from the internuclear distances of $R_{\rm equ}$ to R_ω in the one-photon and net-two-photon dissociation pathways. Further measurements in the isotope D_2 confirm our findings, again, the bond stretching time is found to be the same for the two dissociative ionization pathways of D_2^+ but scaled up by a factor of $\sqrt{2}$ as compared to that of H_2^+.

To acquire an intuitive picture of the timing of the two dissociation pathways of H_2^+, we use a classical mechanics to model the propagation of the nuclear wave packets on the related potential energy curves by solving the Newtonian equations. In order to match the ultimate KER of the nuclear fragments measured in the experiment, the initial kinetic energies of 1.19 and 0.12 eV are assigned for the one-photon and net-two-photon dissociation pathways, which corresponds to the nuclear wave packets launched around $R_{\rm equ}$ and composed of vibrational states centered at $\nu = 9$ and $\nu = 3$ [indicated by the dashed horizontal lines in Fig. 1(a)]. As shown in Fig. 1(b), the nuclear wave packets of the one-photon and net-two-photon pathways take $\tau_{\omega H} = 12.1$ and $\tau_{(3-1)\omega H} = 12.6$ fs to reach R_ω from $R_{\rm equ}$, respectively. Although starting with a lower speed at $R_{\rm equ}$, the bond stretching of the net-two-photon pathway speeds up after absorbing three photons at $R_{3\omega}$ and catches up the one-photon pathway at R_ω.

We performed the experimental measurement in an ultrahigh vacuum chamber using the COLd Target Recoil Ion Momentum Spectrometer (COLTRIMS) technique [36,37], where the photoelectrons and ions produced from the strong-field dissociative ionization of H_2/D_2 were detected in coincidence by two position-sensitive microchannel plate detectors at the opposite ends of the spectrometer. By measuring the time of flight and positions of the charged particle impacts, the three-dimensional momenta and kinetic energies of the photoelectrons and ions were reconstructed event-by-event during the offline analysis. The polarization-skewed laser pulse (rotating red curve) is sketched in Fig. 2(a). The polarization of the electric field $\boldsymbol{E}(t)$ slowly rotates from $\phi_E = 90°$ $(-90°)$ to $\phi_E = 0°$ $(-180°)$ as the time t increases [38,39] (see Supplemental Material [40] on the implementation of the polarization-skewed laser pulse). Here ϕ_E represents the polarization direction of the electric laser field (all the angles are defined with respect to the horizontal y axis, and the lab frame is used throughout this Letter). The vector potential $\boldsymbol{A}(t) = -\int_{-\infty}^{t} \boldsymbol{E}(t')dt'$ shares a similar profile with $\boldsymbol{E}(t)$. Interestingly, for the slowly varying envelope approximation, the $\boldsymbol{A}(t)$ points to the same or opposite direction as that of the $\boldsymbol{E}(t)$, i.e.,$\phi_A(t) = \phi_E(t)(\text{or}+180°) = \arctan\{\exp[-4\ln 2(\Delta t/\tau^2)(t - \frac{1}{2}\Delta t)]\}$. The laser field can be treated as linear polarization within each optical cycle, but the overall polarization direction rotates by 90° from the leading edge to the tail of the pulse. The unique mapping between the cycle-changing polarization direction $\phi_E(t)$ [or $\phi_A(t)$] and its evolution time t makes the polarization-skewed laser pulse a stopwatch to clock the dissociative ionization process (see the mapping curve in Fig. S1 in the Supplemental Material [40]).

Figures 2(b) and 2(c) display the measured momentum distributions of the photoelectrons and the correlated nuclear fragments H^+ of the $H_2(1,0)$ channel. As shown in Fig. 2(c), two sets of nuclear fragments H^+ corresponding to the one-photon and net-two-photon pathways are distinct in their KERs and emission angles $\phi_{\rm ion}$. The corresponding KER spectrum is sketched in the inset of Fig. 1(a). We first investigate the one-photon dissociation pathway by selecting the events within 0.6 eV < KER < 0.75 eV [highlighted in red in the inset of Fig. 1(a), or the inner red ring in Fig. 2(c)]. As indicated by the arc-shaped black arrow in Fig. 2(a), once the H_2 is oriented along

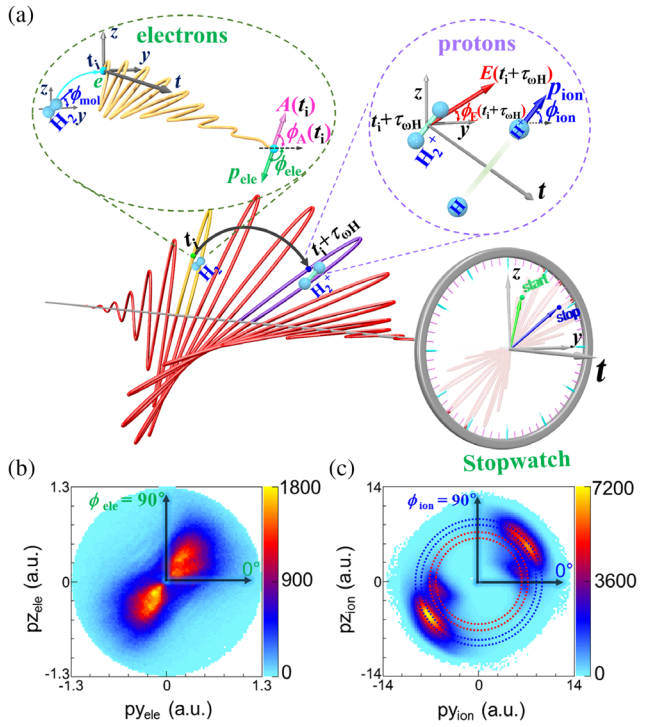

FIG. 2. (a) The sketch of the stopwatch using a polarization-skewed laser pulse (red rotating curve). The yellow curve in the "electrons" inset illustrates the trajectory of the photoelectron emitted from H_2 at ionization instant t_i. Driven by the remaining laser field after t_i, the ultimate momentum of the photoelectron is given by the vector potential $\boldsymbol{A}(t_i)$ at the ionization instant, i.e., $\phi_{\rm ele} = \phi_A + 180°$. As illustrated in the "protons" inset, the stretched H_2^+ transits to the excited state at instant $t_i + \tau_{\omega H}$, where the dipole-transition rate depends on the strength and orientation of the instantaneous laser field $\boldsymbol{E}(t_i + \tau_{\omega H})$ with respect to the molecular orientation $\phi_{\rm mol}$. The $\phi_{\rm mol}$ is read from the measured emission direction of the ejected H^+, i.e., $\phi_{\rm mol} = \phi_{\rm ion}$. (b),(c) Measured momentum distributions of the photoelectrons and correlated nuclear fragments H^+ produced from the $H_2(1,0)$ channel. The events within the dashed red and blue rings in (c) are selected to observe the bond stretching time of the one-photon and net-two-photon dissociation pathways.

the $\phi_{\rm mol}$ direction, and it is ionized at t_i, the stopwatch is triggered. As the H_2^+ bond stretches to R_ω at $t_i + \tau_{\omega H}$, the dipole-transition happens, and the stopwatch stops. The probability of observing a dissociative ionization event can be expressed as $P_{\rm id}(t_i, \phi_{\rm mol}) = P_i(t_i, \phi_{\rm mol}) P_{\omega d}(t_i + \tau_{\omega H}, \phi_{\rm mol})$, where $P_i(t_i, \phi_{\rm mol})$ and $P_{\omega d}(t_i + \tau_{\omega H}, \phi_{\rm mol})$ stand for the ionization rate of H_2 at t_i and the one-photon dipole-transition rate at $t_i + \tau_{\omega H}$, respectively. Driven by a Gaussian-shaped laser pulse, for molecules oriented along $\phi_{\rm mol}$, the envelope of $P_i(t)$, $P_{\omega d}(t)$, and $P_{\rm id}(t)$ can be modeled by Gaussian distributions of $\sim \exp[-(t - t_s)^2/\sigma_s^2]$ centered at t_s with a width of σ_s. Here the (t_s, σ_s) stands for (t_{si}, σ_{si}), $(t_{s\omega d}, \sigma_{s\omega d})$, and $(t_{\rm sid}, \sigma_{\rm sid})$ of the Gaussian profiles of $P_i(t)$, $P_{\omega d}(t)$, and $P_{\rm id}(t)$, respectively. By expressing the Gaussian-shaped $P_{\rm id}(t_i)$ with the product of $P_i(t_i)$ and $P_{\omega d}(t_i + \tau_{\omega H})$, the bond stretching time $\tau_{\omega H}$ of the one-photon pathway can be extracted as

$$\tau_{\omega H} = (t_{s\omega d} - t_{\rm sid}) + (t_{\rm si} - t_{\rm sid}) \frac{\sigma_{s\omega d}^2}{\sigma_{\rm si}^2}. \quad (1)$$

(see the Supplemental Material [40] for details).

The dashed green circle on top of the t_i time in Fig. 2(a) shows the corresponding electron trajectory. The photoelectron released at t_i is drifted by the remaining laser field, and its final momentum is $\boldsymbol{p}_{\rm ele} = -\boldsymbol{A}(t_i)$ if the Coulomb interaction is negligible. Therefore, the emission direction of the photoelectron can be approximated as $\phi_{\rm ele} = \phi_A + 180°$, which allows us to read the ionization instant from the ejected photoelectron by mapping its emission direction to t_i according to the spatiotemporal property of the polarization-skewed laser pulse (see the mapping curve in Fig. S1 in the Supplemental Material [40]). On the other hand, the dashed purple circle on top of the $t_i + \tau_{\omega H}$ in Fig. 2(a) shows that the dissociative protons emitted along $\phi_{\rm mol}$ direction for the one-photon dipole transition at $t_i + \tau_{\omega H}$. We can read the molecular orientation ($\phi_{\rm mol}$) from the measured emission direction of H^+ ($\phi_{\rm ion}$), i.e., $\phi_{\rm mol} = \phi_{\rm ion}$, since the rotation of the molecule is negligible within the ultrafast dissociation process on the femtosecond timescale.

In the following, we select the molecules oriented within $25° < \phi_{\rm mol} < 45°$ to observe and compare the bond stretching time of the one-photon and net-two-photon dissociation pathways directly. In this angle range, these two pathways both have sufficient yields, and our stopwatch has a good time resolution (see the Supplemental Material [40] for more details). As an example, Figs. 3(a) and 3(b) display the photoelectron momentum and angular distributions of the one-photon dissociation pathway for molecules oriented along the direction $\phi_{\rm mol} = 40°$ by selecting the events within $39° < \phi_{\rm ion} < 41°$. The yield of the correlatively measured photoelectrons corresponds to the observed probability of the dissociative single ionization process, which is the product of the photoionization and dipole-transition rates. By relating the $\phi_{\rm ele}$ to the ionization instant t_i, the angular distribution of photoelectrons in Fig. 3(b) is transformed into the distribution of the time-dependent probability $P_{\rm id}(t_i)$, as plotted in Fig. 3(c) (red circles). The measured $P_{\rm id}(t_i)$ can be fitted to a Gaussian function (solid red curve), where we obtain $t_{\rm sid} \sim 5.8$ fs. The ionization rate $P_i(t)$ of H_2 is calculated using the molecular Ammosov-Delone-Krainov (MO-ADK) theory [42,43], where the cycle-changing polarization of the polarization-skewed laser field is adopted. The MO-ADK calculation shows a weak dependence on the molecular orientation [44]. The one-photon dipole-transition rate at R_ω is obtained according to $P_{\omega d}(t) \propto [\boldsymbol{D}(R_\omega)\boldsymbol{E}(t)]^2 \propto E^2(t)\cos^2[\phi_E(t) - \phi_{\rm mol}]$ [45,46], where $\boldsymbol{D}$ is the coupling matrix of the dipole transition. For a molecule oriented

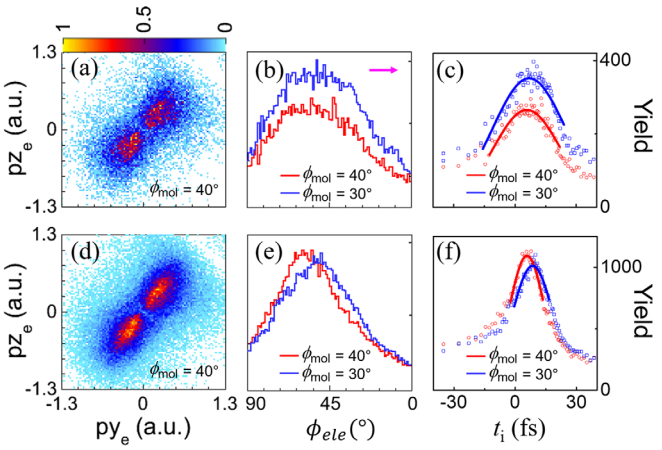

FIG. 3. (a) The photoelectron momentum distribution of the one-photon dissociative ionization pathway of H_2 correlated with molecules oriented along $\phi_{\rm mol} = 40°$. (b) The angular distributions of photoelectrons emitted from molecules oriented along $\phi_{\rm mol} = 40°$ (red curve) and 30° (blue curve). The pink arrow indicates the rotating direction of the polarization of the laser field. (c) The corresponding dissociative ionization probabilities $P_{\rm id}(t_i)$ deduced from the photoelectron angular distributions in (b) by relating $\phi_{\rm ele}$ to the ionization instant t_i. (b) Shares the same vertical axis as (c), which represents the yield of photoelectrons as labeled in the right of (c). (d)–(f) The same as (a)–(c) but for the net-two-photon dissociative ionization pathway of H_2.

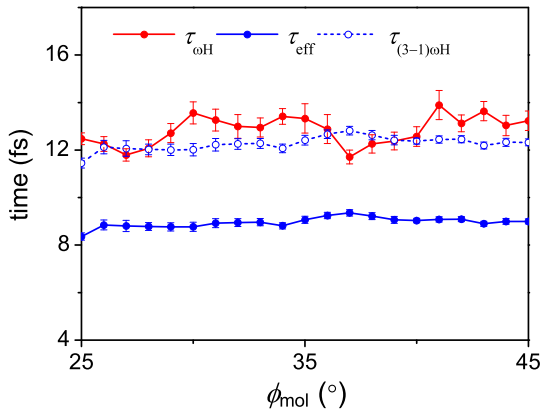

FIG. 4. Experimentally extracted bond stretching time of different dissociation pathways of H_2 as a function of the molecular orientation $\phi_{\rm mol}$. The curve with red circles shows $\tau_{\omega H}$ of the one-photon pathway of H_2. The blue solid and open circle curves are the effective bond stretching times of $\tau_{\rm eff}$ and $\tau_{(3-1)\omega H}$ of the net-two-photon pathway of H_2, respectively.

along $\phi_{\rm mol}$, the ionization and dipole-transition rates can be calculated individually according to the specific spatiotemporal profile of the laser field used in the experiment. For instance for $\phi_{\rm mol} = 40°$, fitting numerically the time-dependent distributions of $P_i(t)$ and $P_{\omega d}(t)$ with Gaussian functions, we obtain $t_{\rm si} \sim 12.1$, $\sigma_{si} \sim 25.3$, $t_{s\omega d} \sim 13.5$, and $\sigma_{s\omega d} \sim 22.2$ fs. By putting all these parameters into Eq. (1), the bond stretching time of the one-photon dissociation pathway is found to be $\tau_{\omega H} = 12.5$ fs (see the Supplemental Material [40] for more details). Similarly, by selecting the events in the range of $29° < \phi_{\rm ion} < 31°$, the corresponding photoelectron angular distribution and $P_{\rm id}(t_i)$ are plotted in Figs. 3(b) and 3(c) (blue curves and squares), from which the bond stretching time is found to be $\tau_{\omega H} = 13.4$ fs.

The pink arrow in Fig. 3(b) marks the rotation direction of the polarization-skewed laser field. The blue curve is slightly shifted along the direction of the arrow as compared to the red one, which indicates that the angular distribution of the correlated photoelectrons rotates as the molecular orientation changes (see the animated movies in the Supplemental Material [40]). For molecules oriented along different directions, the ionization and dipole-transition times may shift along the time axis of the laser pulse. As the polarization direction $\phi_E(t)$ of our laser field does not vary linearly with the evolution time t (see the mapping curve in Fig. S1 in the Supplemental Material [40]), the cross angle between the photoelectron emission direction and the ion emission direction also varies for molecules oriented along different angles. However, the bond stretching time is an inherent property of the ultrafast dissociation process and does not change for different molecular orientations. As plotted in Fig. 4 (solid red circles), the extracted bond stretching time remains the same for molecules oriented along various directions with an averaged time of $\tau_{\omega H} = 12.8 \pm 0.6$ fs, which agrees well with the predicted 12.1 fs in our classical simulation.

For the net-two-photon dissociation pathway, the H_2 oriented along $\phi_{\rm mol}$ is ionized at t_i, after which the newborn H_2^+ takes $\tau_{3\omega H}$ to stretch from $R_{\rm equ}$ to $R_{3\omega}$ and absorbs three photons at $t_i + \tau_{3\omega H}$, followed by emitting one photon at R_ω at $t_i + \tau_{(3-1)\omega H}$. The three-photon up-transition rate at $R_{3\omega}$ is given by $P_{3\omega d}(t) \propto [\boldsymbol{D}(R_{3\omega}) \cdot \boldsymbol{E}(t)]^6 \propto E^6(t) \cos^6[\phi_E(t) - \phi_{\rm mol}]$, while the one-photon down-transition rate at R_ω is $P_{\omega d}(t) \propto [\mathbf{D}(R_\omega) \cdot \boldsymbol{E}(t)]^2 \propto E^2(t) \cos^2[\phi_E(t) - \phi_{\rm mol}]$ [45,46]. Comparing the expressions of $P_{3\omega d}(t)$ and $P_{\omega d}(t)$, one can find that $P_{3\omega d}(t)$ can also be modeled by a Gaussian distribution with $t_{s3\omega d} = t_{s\omega d}$ and $\sigma_{s3\omega d} = \sqrt{3}\sigma_{s\omega d}/3$. The overall dipole-transition rate is weighted by the product of these two rates, i.e., $P_{3\omega d}(t_i + \tau_{3\omega H}) P_{\omega d}(t_i + \tau_{(3-1)\omega H})$ [45,46]. Similar to the one-photon pathway, the overall dipole-transition rate of the net-two-photon pathway can also be expressed using an effective rate of $P_{\rm deff}(t_i + \tau_{\rm eff}) = \exp[-(t_i + \tau_{\rm eff} - t_{s\omega d})^2/\sigma_{\rm seff}^2]$, from which we deduce $\tau_{\rm eff} = 0.75\tau_{3\omega H} + 0.25\tau_{(3-1)\omega H}$ and $\sigma_{\rm seff} = 0.5\sigma_{s\omega d}$. Here the $\tau_{\rm eff}$ can be regarded as the effective bond stretching time of the net-two-photon pathway normalized by the number of photons (see the Supplemental Material [40] for details). Thus the probability of the net-two-photon dissociative ionization pathway is given by $P_{id}(t_i) \propto P_i(t_i) P_{\rm deff}(t_i + \tau_{\rm eff})$, which has a similar formalism with the one-photon dissociation pathway, and the derived $\tau_{\rm eff}$ is

$$\tau_{\mathrm{eff}} = (t_{s\omega d} - t_{\mathrm{sid}}) + (t_{\mathrm{si}} - t_{\mathrm{sid}})\frac{\sigma_{\mathrm{seff}}^2}{\sigma_{\mathrm{si}}^2}. \quad (2)$$

For the net-two-photon dissociation pathway, we experimentally select the events of 1.2 eV < KER < 1.35 eV [highlighted in blue in the inset of Fig. 1(a), or the outer blue ring in Fig. 2(c)]. The measured momentum and angular distributions of the photoelectrons of the net-two-photon pathway are shown in Figs. 3(d)–3(f) for molecules oriented along $\phi_{\mathrm{mol}} = 30°$ and 40°. The solid blue circles in Fig. 4 display the effective bond stretching time for various molecular orientations with an average value of $\tau_{\mathrm{eff}} = 9.0 \pm 0.2$ fs, which is in good agreement with the classical effective bond stretching time of 9.2 fs, affirming the reliability of our classical model. By considering the ratio $\gamma = \tau_{3\omega H}/\tau_{(3-1)\omega H} = 0.64$ obtained from the classical model, the deduced $\tau_{(3-1)\omega H}$ is shown in Fig. 4 (open blue circles) with an average value of $\tau_{(3-1)\omega H} = 12.3 \pm 0.3$ fs. Our measurements indicate that the one-photon and net-two-photon dissociation pathways take almost the same time to stretch to R_ω after the photoionization.

The similar bond stretching time for the one-photon and net-two-photon pathways is further confirmed in the dissociative ionization of D_2. Our results show that the D_2^+ has a bond stretching time of $\tau_{\omega D} = 17.4 \pm 0.6$ fs and $\tau_{(3-1)\omega D} = 18.8 \pm 0.2$ fs in the same measurement using a 1:1 gas mixture of H_2 and D_2 (see the Supplemental Material [40] for details), which is slightly different from the numerically predicted values of $\tau_{\omega D} = 17.2$ and $\tau_{(3-1)\omega D} = 17.8$ fs. Such a difference might be due to the relatively long bond stretching time of D_2^+ as compared to that of H_2^+. As a result, either the ionization or the dipole-transition between $1s\sigma_g^+$ and $2p\sigma_u^+$ states of D_2^+ will occur at the rising or falling edges of the laser pulse, where the polarization direction $\phi_E(t)$ is less sensitive to the change of the evolution time t and thus may introduce relatively large errors in the experiment. For the same photon-resolved dissociation pathway, the bond stretching time of D_2^+ is $\sqrt{2}$ times of that of H_2^+, which is indeed expected since the nuclear mass of D_2 is twice that of H_2. The extracted data from the D_2 experiment confirm the robustness and capability of the ultrafast stopwatch method.

In conclusion, we experimentally clock the bond stretching process of the dissociative ionization of hydrogen molecules using a stopwatch of a polarization-skewed femtosecond laser pulse. By reading the photoionization and dipole-transition instants from the angular distributions of the ejected photoelectrons and nuclear fragments, we find that the bond stretching time of the one-photon and net-two-photon pathways are almost equal. The ultrafast stopwatch strategy using a polarization-skewed laser pulse provides a straightforward and robust tool to probe the ultrafast dynamics with ultrahigh time resolution, which opens new possibilities to explore ultrafast processes in molecules.

This work was supported by the National Key R&D Program of China (Grants No. 2018YFA0306303 and No. 2018YFA0404802); the National Natural Science Fund (Grants No. 11425416, No. 61690224, No. 11834004, No. 11621404, No. 11704124, No. 11574205, No. 11721091, and No. 91850203); the 111 project of China (Grant No. B12024); Projects from Shanghai Science and Technology Commission (19JC1412200); Innovation Program of Shanghai Municipal Education Commission (2017-01-07-00-02-E00034), and Shanghai Shuguang Project (17SG10).

*fhe@sjtu.edu.cn
†jwu@phy.ecnu.edu.cn

[1] M. F. Kling, C. Siedschlag, A. J. Verhoef, J. I. Khan, M. Schultze, T. Uphues, Y. Ni, M. Uiberacker, M. Drescher, F. Krausz, and M. J. J. Vrakking, Science **312**, 246 (2006).
[2] J. Wu, M. Magrakvelidze, L. P. H. Schmidt, M. Kunitski, T. Pfeifer, M. Schöffler, M. Pitzer, M. Richter, S. Voss, H. Sann, H. Kim, J. Lower, T. Jahnke, A. Czasch, U. Thumm, and R. Dörner, Nat. Commun. **4**, 2177 (2013).
[3] H. Xu, Z. Li, F. He, X. Wang, A. Atia-Tul-Noor, D. Kielpinski, R. T. Sang, and I. V. Litvinyuk, Nat. Commun. **8**, 15849 (2017).
[4] F. Martín, J. Fernández, T. Havermeier, L. Foucar, T. Weber, K. Kreidi, M. Schöffler, L. Schmidt, T. Jahnke, O. Jagutzki, A. Czasch, E. P. Benis, T. Osipov, A. L. Landers, A. Belkacem, M. H. Prior, H. Schmidt-Böcking, C. L. Cocke, and R. Dörner, Science **315**, 629 (2007).
[5] F. He, A. Becker, and U. Thumm, Phys. Rev. Lett. **101**, 213002 (2008).
[6] M. Kremer, B. Fischer, B. Feuerstein, V. L. B. de Jesus, V. Sharma, C. Hofrichter, A. Rudenko, U. Thumm, C. D. Schröter, R. Moshammer, and J. Ullrich, Phys. Rev. Lett. **103**, 213003 (2009).
[7] D. Ray, F. He, S. De, W. Cao, H. Mashiko, P. Ranitovic, K. P. Singh, I. Znakovskaya, U. Thumm, G. G. Paulus, M. F. Kling, I. V. Litvinyuk, and C. L. Cocke, Phys. Rev. Lett. **103**, 223201 (2009).
[8] A. González-Castrillo, A. Palacios, H. Bachau, and F. Martín, Phys. Rev. Lett. **108**, 063009 (2012).
[9] I. Znakovskaya, P. von den Hoff, G. Marcus, S. Zherebtsov, B. Bergues, X. Gu, Y. Deng, M. J. J. Vrakking, R. Kienberger, F. Krausz, R. de Vivie-Riedle, and M. F. Kling, Phys. Rev. Lett. **108**, 063002 (2012).
[10] Z. Wang, K. Liu, P. Lan, and P. Lu, Phys. Rev. A **91**, 043419 (2015).
[11] T. Zuo and A. D. Bandrauk, Phys. Rev. A **52**, R2511 (1995).
[12] D. M. Villeneuve, M. Y. Ivanov, and P. B. Corkum, Phys. Rev. A **54**, 736 (1996).
[13] X.-B. Bian, L.-Y. Peng, and T.-Y. Shi, Phys. Rev. A **77**, 063415 (2008).
[14] E. Dehghanian, A. D. Bandrauk, and G. L. Kamta, Phys. Rev. A **81**, 061403(R) (2010).
[15] H. He, R. Lu, P. Zhang, Y. Guo, K. Han, and G. He, Phys. Rev. A **84**, 033418 (2011).
[16] A. Picón, A. Jaroń-Becker, and A. Becker, Phys. Rev. Lett. **109**, 163002 (2012).

[17] C. B. Madsen, F. Anis, L. B. Madsen, and B. D. Esry, Phys. Rev. Lett. **109**, 163003 (2012).
[18] R. E. F. Silva, F. Catoire, P. Rivière, H. Bachau, and F. Martín, Phys. Rev. Lett. **110**, 113001 (2013).
[19] J. Wu, M. Kunitski, M. Pitzer, F. Trinter, L. P. H. Schmidt, T. Jahnke, M. Magrakvelidze, C. B. Madsen, L. B. Madsen, U. Thumm, and R. Dörner, Phys. Rev. Lett. **111**, 023002 (2013); W. Zhang, Z. Li, P. Lu, X. Gong, Q. Song, Q. Ji, K. Lin, J. Ma, F. He, H. Zeng, and J. Wu, Phys. Rev. Lett. **117**, 103002 (2016); P. Lu, J. Wang, H. Li, K. Lin, X. Gong, Q. Song, Q. Ji, W. Zhang, J. Ma, H. Li, H. Zeng, F. He, and J. Wu, Proc. Natl. Acad. Sci. U.S.A. **115**, 2049 (2018).
[20] K. Liu, P. Lan, C. Huang, Q. Zhang, and P. Lu, Phys. Rev. A **89**, 053423 (2014).
[21] B. Manschwetus, T. Nubbemeyer, K. Gorling, G. Steinmeyer, U. Eichmann, H. Rottke, and W. Sandner, Phys. Rev. Lett. **102**, 113002 (2009).
[22] W. Zhang, Z. Yu, X. Gong, J. Wang, P. Lu, H. Li, Q. Song, Q. Ji, K. Lin, J. Ma, H. Li, F. Sun, J. Qiang, H. Zeng, F. He, and J. Wu, Phys. Rev. Lett. **119**, 253202 (2017); W. Zhang, X. Gong, H. Li, P. Lu, F. Sun, Q. Ji, K. Lin, J. Ma, H. Li, J. Qiang, F. He, and J. Wu, Nat. Commun. **10**, 757 (2019).
[23] D. Akoury *et al.*, Science **318**, 949 (2007).
[24] A. Picón, A. Bahabad, H. C. Kapteyn, M. M. Murnane, and A. Becker, Phys. Rev. A **83**, 013414 (2011).
[25] H. Niikura, F. Légaré, R. Hasbani, A. D. Bandrauk, M. Y. Ivanov, D. M. Villeneuve, and P. B. Corkum, Nature (London) **417**, 917 (2002).
[26] A. S. Alnaser, X. M. Tong, T. Osipov, S. Voss, C. M. Maharjan, P. Ranitovic, B. Ulrich, B. Shan, Z. Chang, C. D. Lin, and C. L. Cocke, Phys. Rev. Lett. **93**, 183202 (2004).
[27] A. Staudte, D. Pavičić, S. Chelkowski, D. Zeidler, M. Meckel, H. Niikura, M. Schöffler, S. Schössler, B. Ulrich, P. P. Rajeev, T. Weber, T. Jahnke, D. M. Villeneuve, A. D. Bandrauk, C. L. Cocke, P. B. Corkum, and R. Dörner, Phys. Rev. Lett. **98**, 073003 (2007).
[28] A. Giusti-Suzor, X. He, O. Atabek, and F. H. Mies, Phys. Rev. Lett. **64**, 515 (1990).
[29] A. H. Zewail, Science **242**, 1645 (1988).
[30] C. E. Crespo-Hernández, B. Cohen, and B. Kohler, Nature (London) **436**, 1141 (2005).
[31] T. Ergler, A. Rudenko, B. Feuerstein, K. Zrost, C. D. Schröter, R. Moshammer, and J. Ullrich, Phys. Rev. Lett. **97**, 193001 (2006).
[32] S. Larimian, S. Erattupuzha, S. Mai, P. Marquetand, L. González, A. Baltuška, M. Kitzler, and X. Xie, Phys. Rev. A **95**, 011404(R) (2017).
[33] P. Eckle, A. N. Pfeiffer, C. Cirelli, A. Staudte, R. Dörner, H. G. Muller, M. Büttiker, and U. Keller, Science **322**, 1525 (2008).
[34] L. Holmegaard, J. L. Hansen, L. Kalhøj, S. Louise Kragh, H. Stapelfeldt, F. Filsinger, J. Küpper, G. Meijer, D. Dimitrovski, M. Abu-samha, C. P. J. Martiny, and L. Bojer Madsen, Nat. Phys. **6**, 428 (2010).
[35] A. N. Pfeiffer, C. Cirelli, M. Smolarski, R. Dörner, and U. Keller, Nat. Phys. **7**, 428 (2011).
[36] J. Ullrich, R. Moshammer, A. Dorn, R. Dörner, L. P. H. Schmidt, and H. Schmidt-Böcking, Rep. Prog. Phys. **66**, 1463 (2003).
[37] R. Dörner, V. Mergel, O. Jagutzki, L. Spielberger, J. Ullrich, R. Moshammer, and H. Schmidt-Böcking, Phys. Rep. **330**, 95 (2000).
[38] G. Karras, M. Ndong, E. Hertz, D. Sugny, F. Billard, B. Lavorel, and O. Faucher, Phys. Rev. Lett. **114**, 103001 (2015).
[39] Q. Ji, J. Wang, P. Lu, H. Li, X. Gong, Q. Song, K. Lin, W. Zhang, J. Ma, M. F. Kling, H. Zeng, J. Wu, and F. He, Phys. Rev. A **96**, 053423 (2017).
[40] See Supplemental Material at http://link.aps.org/supplemental/10.1103/PhysRevLett.123.233202 for the animated movies of the rotating photoelectron momentum distributions as a function of molecular orientation, details on experimental construction of the polarization-skewed laser pulse, and the data analysis to extract the bond stretching time of H_2^+ and D_2^+, which includes Ref. [41].
[41] M. Magrakvelidze, F. He, S. De, I. Bocharova, D. Ray, U. Thumm, and I. V. Litvinyuk, Phys. Rev. A **79**, 033408 (2009).
[42] X. M. Tong, Z. X. Zhao, and C. D. Lin, Phys. Rev. A **66**, 033402 (2002).
[43] S.-F. Zhao, C. Jin, A.-T. Le, T. F. Jiang, and C. D. Lin, Phys. Rev. A **81**, 033423 (2010).
[44] A. Staudte, S. Patchkovskii, D. Pavičić, H. Akagi, O. Smirnova, D. Zeidler, M. Meckel, D. M. Villeneuve, R. Dörner, M. Yu. Ivanov, and P. B. Corkum, Phys. Rev. Lett. **102**, 033004 (2009).
[45] A. M. Sayler, P. Q. Wang, K. D. Carnes, B. D. Esry, and I. Ben-Itzhak, Phys. Rev. A **75**, 063420 (2007).
[46] X. Gong, P. He, Q. Song, Q. Ji, H. Pan, J. Ding, F. He, H. Zeng, and J. Wu, Phys. Rev. Lett. **113**, 203001 (2014).